The 9th European Congress on Computational Methods in Applied Sciences and Engineering
ECCOMAS Congress 2024
3–7 June 2024, Lisboa, Portugal

LARGE ROTATION ISOGEOMETRIC SHELL MODEL FOR ALTERNATING STIFF/SOFT CURVED LAMINATES INCLUDING WARPING AND THICKNESS STRAIN WITH MINIMAL DOFS

L. LEONETTI[12], D. MAGISANO[1] and G. GARCEA[1]

[1] Department of Informatics, Modeling, Electronics and Systems Engineering (DIMES)
University of Calabria
87036 Rende (Cosenza), Italy

[2] CIRTech Institute
HUTECH University
Ho Chi Minh City, Vietnam

Key words: Layered structures, shell, solid-shell, finite element method, buckling, geometric nonlinearity.

Summary. The behaviour of laminates with alternating elastic stiff and soft layers is characterized by the concentration of transverse shear deformations in the soft layers with significant zigzag warping effects while membrane and bending actions are borne by the hard layers. Curved geometry and large deformations can induce interlayer thickness strain, affecting the laminate's overall response. This work introduces a rotation-free Total Lagrangian curved shell model to accurately capture these structural responses. Each stiff layer is modeled as a Kirchhoff-Love shell, and each soft interlayer as a solid-shell, with interface displacements expressed through the mid-surface displacements of adjoining stiff layers. The model has a sparse stiffness matrix compared to high-order theories and requires only 3 DOFs per stiff layer to replicate the 3D solution. A NURBS discretization ensures high continuity with patch-wise reduced quadrature to avoid locking and enhance efficiency.

1 INTRODUCTION

Composite laminated plates and shells, valued for their strength and lightness, have advanced various engineering fields. These laminates, formed by stacking layers of different materials or plies of the same material with varying orientations, exhibit unique deformation behaviors. A notable example is structural glass [1, 2, 3], which consists of glass plies bonded by soft polymeric interlayers, leading to significant transverse shear strains and zigzag warping effects.

Fully 3D models with finite element discretization through the laminate thickness are versatile but computationally demanding, particularly for nonlinear analyses. Laminated shell theories offer a more efficient alternative, typically classified into equivalent single-layer (ESL) and layer-wise (LW) models.

The classical Kirchhoff-Love theory, suitable for slender structures, neglects transverse shear deformations. First-Order Shear Deformation Theory (FSDT) incorporates these deformations but assumes planar cross-sections post-deformation, limiting its applicability. High-Order Shear

Deformation Theories (HSDT) [4] introduce higher-order thickness terms to model warping but require many unknowns for accuracy. Zigzag Theories (ZZT) [5, 6, 7] enhance FSDT by adding piecewise linear zigzag contributions to in-plane displacements, effectively modeling cross-sectional warping with fewer unknowns. The Refined ZZT (RZZT) [8, 9, 10, 11] is notable for its accuracy, though it relies on the assigned zigzag shape.

LW theories [12, 13, 14, 15] provide quasi-3D displacement descriptions within each layer, ensuring continuity of transverse shear stresses. However, the number of unknowns scales with the number of layers, which can be prohibitive. Recent LW proposals model each lamina as a Kirchhoff-Love shell with spline-based discretization, enabling damage modeling.

A key work on alternating layups is [16], which proposes a shell model that imposes equal rotation on stiff layers while allowing independent shear deformations in soft interlayers. This quasi-LW approach adds only two additional degrees of freedom (DOFs) per soft layer, offering a balance between accuracy and computational efficiency. Inspired by this, [17] developed a Total Lagrangian, rotation-free model that further reduces DOFs but requires spline basis functions for C^1 continuity. The RZZT can also be a viable alternative, using a single zigzag function regardless of the number of layers, but it may falter when layer stiffness ratios are extreme or non-uniform.

Solid-shell models offer another approach, using a 3D continuum model with linear kinematic approximation through the thickness and only displacement DOFs. Homogenized solid-shell models equivalent to FSDT are effective, and LW solid-shell models can capture sectional warping with one element per layer.

The hypothesis of equal rotation for stiff layers has been used in many quasi-LW models for alternating layups, providing reliable predictions for moderately curved structures with moderate rotations. However, for highly curved laminates or those undergoing large deformations, this constraint can reduce model accuracy. Thickness deformations in soft interlayers can induce significant differences in the bending rotations of stiff layers, leading to errors in models that neglect this behavior.

This work advances existing proposals by presenting a hybrid model combining large deformation Kirchhoff-Love shell theory with a solid-shell approach, aiming for a robust and efficient formulation for alternating curved laminates under finite deformation. Each stiff layer is modeled using Kirchhoff-Love hypotheses and NURBS interpolation for high continuity. Soft layers are modeled with a solid-shell formulation, where solid-shell variables are derived from the mid-surface displacements of the coupled stiff layers. This approach ensures a high-continuity approximation without additional unknowns.

The model is nearly a full 3D description, with the Kirchhoff-Love assumption for stiff layers. It uses only 3 DOFs per stiff layer for each control point and benefits from C^2 cubic NURBS displacement approximation, reducing the number of control points needed for accuracy. A patch-wise numerical integration scheme eliminates membrane and shear locking, using few integration points for enhanced computational efficiency. This formulation is ideal for alternating laminated structures with significant curvatures, offering reliability and a small number of unknowns. Compared to HSDT and multi-warping function models, it yields a sparse stiffness matrix and maintains high efficiency.

The paper is structured as follows: Section 2 describes the new laminated shell model theory, Section 3 covers its effective isogeometric discretization, Section 4 presents numerical tests validating the proposal, and the final section offers conclusions.

2 THe ALTERNATING STIFF/SOFT LAMINATED MODEL

2.1 General introduction and fundamental hypotheses

The central idea of the proposed model for alternating laminates is a specialized kinematic description that reduces the unknowns of the 3D solution without any loss in accuracy. The fundamental hypotheses of this model, supported by literature results and the present numerical study, can be summarized as follows.

Firstly, each stiff layer behaves as a thin Kirchhoff-Love shell, where transverse shear strains are negligible. The plane stress condition links the thickness strain to the in-plane strains, which are the only active components. Thus, the kinematics of each stiff layer are described solely by the displacement of its mid-surface [18, 19, 20].

Secondly, each soft interlayer, coupling two stiff layers, exhibits significant transverse shear deformations and can undergo notable thickness strain and stress in curved configurations. While the soft interlayer has insignificant bending stiffness on its own, its bonding action significantly influences the overall laminate's bending stiffness. This overall stiffness falls between that predicted by a plane section hypothesis and that corresponding to uncoupled stiff layers, but often closer to the latter. The kinematics of the soft layer are well described by a linear displacement shape through its thickness, controlled by the displacement of its top and bottom surfaces, similar to a solid-shell model [21, 22, 23].

Lastly, the displacement field is C^0 continuous across layers. This continuity is achieved by expressing the top and bottom displacements of each soft layer as a nonlinear function of the mid-surface displacement (and its in-plane derivatives) of the top and bottom stiff layers it couples, according to the exact finite Kirchhoff-Love kinematics. This approach allows for accurate modeling of the zigzag warping of the laminate section as well as the thickness change of the interlayers. These hypotheses ensure that the proposed model can accurately capture the complex behavior of alternating laminates while maintaining computational efficiency.

2.2 Kinematics

For each layer, a set of convective coordinates ξ^α (where $\alpha = 1, 2$) is defined over its mid-surface, which is assumed, without loss of generality, to be the reference shell surface. In the thickness direction, the coordinate ξ^3 is used, with its bounds representing the offsets of bottom and top surfaces of the layer relative to the reference surface.

We assume that the reference surface of each layer in the initial configuration is an offset of the reference surface of the entire laminate. Thus, points with the same ξ^α (where $\alpha = 1, 2$) but on different layers initially lie on the same normal segment, defining the laminate's geometry.

The position of material points $\mathbf{x}(\xi^1, \xi^2, \xi^3)$ in the current configuration (see Fig. 1) is determined by the position vector $\mathbf{X}(\xi^1, \xi^2, \xi^3)$ in the reference configuration and the displacement $\mathbf{d}(\xi^1, \xi^2, \xi^3)$:

$$\mathbf{x}(\xi^1, \xi^2, \xi^3) = \mathbf{X}(\xi^1, \xi^2, \xi^3) + \mathbf{d}(\xi^1, \xi^2, \xi^3). \tag{1}$$

The covariant basis vectors in the undeformed configuration are derived from the corresponding partial derivatives $\mathbf{G}_i \equiv \frac{\partial \mathbf{X}}{\partial \xi^i} = \mathbf{X}_{,i}$, where $i = 1, 2, 3$, of the position vectors $\mathbf{X}$. From this point forward, a comma will indicate a partial derivative with respect to a generic convective coordinate. Given our assumption about the initial geometry, the direction of $\mathbf{G}_3$ remains

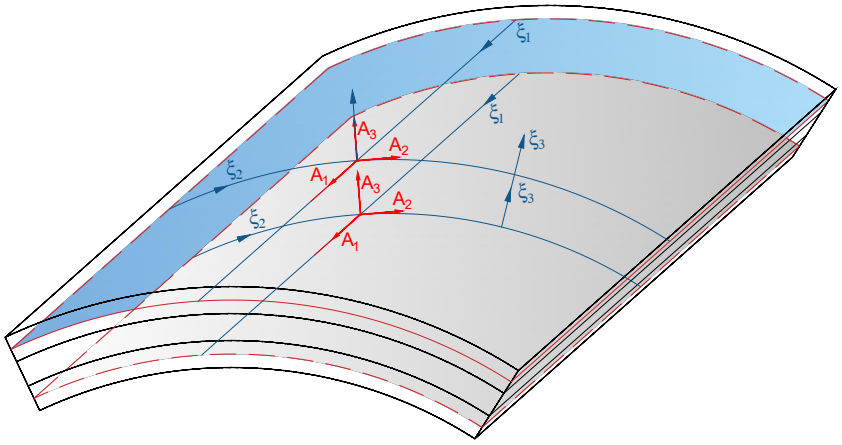

Figure 1: Reference configuration for the laminates and curvilinear coordinates.

consistent across all layers.

Let $\mathbf{G}^i$, where $i = 1, 2, 3$, denote the contravariant basis vectors such that $\mathbf{G}_i \cdot \mathbf{G}^j = \delta_i^j$, with δ_i^j as the Kronecker delta and $(\cdot)$ representing the scalar product. The Green-Lagrange strain tensor can then be expressed in terms of its covariant components $\bar{E}_{ij}$ as

$$\mathbf{E}_{GL} = \sum_{i,j=1}^{3} \bar{E}_{ij}\, \mathbf{G}^i \otimes \mathbf{G}^j \quad \text{with} \quad \bar{E}_{ij} = \frac{1}{2}\left(\mathbf{d}_i \cdot \mathbf{G}_j + \mathbf{d}_j \cdot \mathbf{G}_i + \mathbf{d}_i \cdot \mathbf{d}_j\right) \tag{2}$$

where $(\otimes)$ is used for tensor product.

2.3 Kirchhoff-Love model for hard layers

The position $\mathbf{x}$ of shell points in the current configuration is

$$\mathbf{x} = \mathbf{r}(\xi^1, \xi^2) + \xi^3 \mathbf{a}_3(\xi^1, \xi^2) \tag{3}$$

where $\xi^3 \in [-h/2, h/2]$, with h being the layer thickness. Here $\mathbf{r}(\xi^1, \xi^2) = \mathbf{R}(\xi^1, \xi^2) + \mathbf{u}(\xi^1, \xi^2)$ is the current position of the reference surface, $\mathbf{u}(\xi^1, \xi^2)$ its displacement and $\mathbf{R}(\xi^1, \xi^2)$ represents the position on the reference surface of the considered layers, and $\mathbf{a}_3$ denotes the shell normal, defined as

$$\mathbf{a}_3 = \frac{\mathbf{a}_1 \times \mathbf{a}_2}{|\mathbf{a}_1 \times \mathbf{a}_2|}, \qquad \mathbf{a}_\alpha = \frac{\partial \mathbf{r}}{\partial \xi^\alpha} \quad \text{and} \quad \alpha = 1, 2 \tag{4}$$

The curvatures tensor components[24] are defined as

$$b_{\alpha\beta} = -\frac{1}{2}(\mathbf{a}_\alpha \cdot \mathbf{a}_{3,\beta} + \mathbf{a}_\beta \cdot \mathbf{a}_{3,\alpha}) = \mathbf{a}_{\alpha,\beta} \cdot \mathbf{a}_3 \tag{5}$$

where the reference $\mathbf{a}_\alpha \cdot \mathbf{a}^\beta = \delta_\alpha^\beta$. The covariant basis can be computed over the body by

$$\mathbf{g}_\alpha = \frac{\partial \mathbf{x}}{\partial \xi^\alpha} = \mathbf{a}_\alpha + \xi^3 \mathbf{a}_{3,\alpha} \quad \text{and} \quad \mathbf{g}_3 = \frac{\partial \mathbf{x}}{\partial \xi^3} = \mathbf{a}_3(\xi^1, \xi^2). \tag{6}$$

The current configuration quantities can be obtained by setting $\mathbf{u}(\xi^1,\xi^2)=\mathbf{0}$ and by replacing the basis ($\mathbf{g}$), the normal ($\mathbf{a}_3$) and the curvatures $b_{\alpha\beta}$ with capital letters, $\mathbf{G}$, $\mathbf{A}_3$ and $B_{\alpha\beta}$, respectively.

The displacement of the hard layer is defined as

$$\mathbf{d}=\mathbf{x}-\mathbf{X}=\mathbf{u}(\xi^1,\xi^2)+\xi^3(\mathbf{a}_3(\xi^1,\xi^2)-\mathbf{A}_3(\xi^1,\xi^2)) \tag{7}$$

and its partial derivatives can be obtained as

$$\mathbf{d}_{,\alpha}=\mathbf{u}_{,\alpha}+\xi^3(\mathbf{a}_{3,\alpha}-\mathbf{A}_{3,\alpha}) \qquad \mathbf{d}_{,3}=\mathbf{a}_3(\xi^1,\xi^2)-\mathbf{A}_3(\xi^1,\xi^2)$$

As a result, the transverse shear strains are eliminated, meaning $\bar{E}_{\alpha 3}=0$. By assuming that the strain varies linearly through the thickness, the active strain components can be decomposed into a constant membrane part and a linear bending part. The covariant strain components are:

$$\bar{E}_{\alpha\beta}=\bar{e}_{\alpha\beta}+\xi^3\bar{\chi}_{\alpha\beta}=\frac{1}{2}(a_{\alpha\beta}-A_{\alpha\beta})+\xi^3(B_{\alpha\beta}-b_{\alpha\beta}) \tag{8}$$

with $a_{\alpha\beta}=\mathbf{a}_\alpha\cdot\mathbf{a}_\beta$ and $A_{\alpha\beta}=\mathbf{A}_\alpha\cdot\mathbf{A}_\beta$. Equation (8) defines the covariant membrane strain and curvature components for each hard layer as

$$\bar{e}_{\alpha\beta}=\frac{1}{2}(a_{\alpha\beta}-A_{\alpha\beta}), \qquad \bar{\chi}_{\alpha\beta}=B_{\alpha\beta}-b_{\alpha\beta}.$$

The covariant strains Voigt's notation are collected as

$$\bar{\mathbf{E}}=\bar{\mathbf{e}}+\xi^3\bar{\boldsymbol{\chi}} \quad \text{with} \quad \bar{\mathbf{E}}=\begin{bmatrix}\bar{E}_{11}\\ \bar{E}_{22}\\ 2\bar{E}_{12}\end{bmatrix}, \quad \bar{\mathbf{e}}=\begin{bmatrix}\bar{e}_{11}\\ \bar{e}_{22}\\ 2\bar{e}_{12}\end{bmatrix}, \quad \bar{\boldsymbol{\chi}}=\begin{bmatrix}\bar{\chi}_{11}\\ \bar{\chi}_{22}\\ 2\bar{\chi}_{12}\end{bmatrix}. \tag{9}$$

The term $|\mathbf{a}_1\times\mathbf{a}_2|$ in the denominator of Eq. (4) results in a complex expression for curvature in terms of the displacement field, making the computation of the discrete operators derived from strain differentiation quite expensive. To address this, a simplified formula for curvature, as proposed in [19], is adopted here. This approach leverages the assumption of arbitrarily large deformations but small membrane strains, allowing for the following simplification in the denominator of $\mathbf{a}_3$:

$$|\mathbf{m}|\approx|\mathbf{M}|=\frac{1}{M} \quad \Rightarrow \quad \mathbf{a}_3\approx M\,\mathbf{a}_1\times\mathbf{a}_2. \tag{10}$$

where

$$\mathbf{M}=\mathbf{A}_1\times\mathbf{A}_2 \qquad \mathbf{m}=\mathbf{a}_1\times\mathbf{a}_2,$$

Simplified curvature components, due to (10)

$$\bar{\chi}_{\alpha\beta}=B_{\alpha\beta}-b_{\alpha\beta}\approx M\,(\mathbf{A}_{\alpha,\beta}\cdot(\mathbf{A}_1\times\mathbf{A}_2)-\mathbf{a}_{\alpha,\beta}\cdot(\mathbf{a}_1\times\mathbf{a}_2)) \tag{11}$$

are used in place of Eq. (5) [25]. Moreover, by using (10) into Eq. (4), we have

$$\mathbf{a}_3\approx M\mathbf{m} \quad \Rightarrow \quad \mathbf{a}_{3,\alpha}=M_{,\alpha}\,\mathbf{W}(\mathbf{a}_1)\mathbf{a}_2+M\,(\mathbf{W}(\mathbf{a}_{1,\alpha})\mathbf{a}_2+\mathbf{W}(\mathbf{a}_1)\mathbf{a}_{2,\alpha}) \tag{12}$$

with

$$M_{,\alpha}=-M^3(\mathbf{M}_{,\alpha}\cdot\mathbf{M}) \quad \text{and} \quad \mathbf{a}_{\alpha,\beta}=\mathbf{A}_{\alpha,\beta}+\mathbf{u}_{,\alpha\beta} \quad \alpha=1,2.$$

and where $\mathbf{W}(\mathbf{x})$ represents the spin of vector $\mathbf{x}$.

2.4 Solid shell model for the soft layers

A linear through-the-thickness interpolation is assumed for the position vector

$$\mathbf{X}(\xi^1,\xi^2,\xi^3)=\mathbf{X}_0(\xi^1,\xi^2)+\xi^3\mathbf{X}_n(\xi^1,\xi^2) \tag{13}$$

and for the displacement field

$$\mathbf{d}(\xi^1,\xi^2,\xi^3)=\mathbf{d}_0(\xi^1,\xi^2)+\xi^3\mathbf{d}_n(\xi^1,\xi^2) \tag{14}$$

$\mathbf{d}_0(\xi^1,\xi^2)$ and $\mathbf{d}_n(\xi^1,\xi^2)$ are the semi-sum and semi-difference of the displacements of top and bottom surfaces [21]:

$$\mathbf{d}_0(\xi^1,\xi^2)=\frac{1}{2}\left(\mathbf{d}_t(\xi^1,\xi^2)+\mathbf{d}_b(\xi^1,\xi^2)\right),\qquad \mathbf{d}_n(\xi^1,\xi^2)=\frac{1}{2}\left(\mathbf{d}_t(\xi^1,\xi^2)-\mathbf{d}_b(\xi^1,\xi^2)\right).$$

where the thickness convective coordinate is assumed as $\xi^3\in[-1,1]$. Similarly for the position we have

$$\mathbf{X}_0(\xi^1,\xi^2)=\frac{1}{2}\left(\mathbf{X}(\xi^1,\xi^2,1)+\mathbf{X}(\xi^1,\xi^2,-1)\right),\qquad \mathbf{X}_n(\xi^1,\xi^2)=\frac{1}{2}\left(\mathbf{X}(\xi^1,\xi^2,1)-\mathbf{X}(\xi^1,\xi^2,-1)\right)$$

By utilizing the C^0 continuity across layers, the displacements of the top and bottom surfaces are determined by the displacements of the upper and lower stiff layers (see Fig. 1). Specifically, the displacement of the top surface of the solid-shell layer, in its deformed state, matches that of the overlying stiff layer, as given by Eq. (7) for $\xi^3_t=-h_t/2$, where ξ^3_t represents the thickness coordinate of the top Kirchhoff-Love layer. Similarly, the displacement of the bottom surface is derived from the displacement of the bottom Kirchhoff-Love layer at $\xi^3_b=h_b/2$. Therefore, denoting the quantities corresponding to the top and bottom Kirchhoff-Love layers with the subscripts t and b, respectively, we obtain the following relationship

$$\begin{aligned}\mathbf{d}_t(\xi^1,\xi^2)&=\mathbf{u}_t(\xi^1,\xi^2)+z_t\left(\mathbf{a}_{3t}(\xi^1,\xi^2)-\mathbf{A}_{3t}(\xi^1,\xi^2)\right)\\ \mathbf{d}_b(\xi^1,\xi^2)&=\mathbf{u}_b(\xi^1,\xi^2)+z_b\left(\mathbf{a}_{3b}(\xi^1,\xi^2)-\mathbf{A}_{3b}(\xi^1,\xi^2)\right)\end{aligned} \tag{15}$$

where $z_t=-h_t/2$ and $z_b=h_b/2$. By introducing the Kirchhoff-Love kinematics in Eq. (15) we get

$$\mathbf{d}(\xi^1,\xi^2,\xi^3)=\mathbf{d}^u(\xi^1,\xi^2,\xi^3)+\mathbf{d}^v(\xi^1,\xi^2,\xi^3)\quad\text{with}\quad\begin{aligned}\mathbf{d}^u(\xi^1,\xi^2,\xi^3)&=\mathbf{u}_0(\xi^1,\xi^2)+\xi^3\mathbf{u}_n(\xi^1,\xi^2)\\ \mathbf{d}^v(\xi^1,\xi^2,\xi^3)&=\mathbf{v}_0(\xi^1,\xi^2)+\xi^3\mathbf{v}_n(\xi^1,\xi^2)\end{aligned} \tag{16}$$

Here, the terms $\mathbf{d}^u$ and $\mathbf{d}^v$ correspond to $\mathbf{u}=\{\mathbf{u}_0,\mathbf{u}_n\}$ and $\mathbf{v}=\{\mathbf{v}_0,\mathbf{v}_n\}$, respectively, where the subscripts 0 and n represent the semi-sum and semi-difference of the quantities. Thus, we have

$$\mathbf{u}_0(\xi^1,\xi^2)=\frac{1}{2}\left(\mathbf{u}_t(\xi^1,\xi^2)+\mathbf{u}_b(\xi^1,\xi^2)\right)\qquad \mathbf{u}_n(\xi^1,\xi^2)=\frac{1}{2}\left(\mathbf{u}_t(\xi^1,\xi^2)-\mathbf{u}_b(\xi^1,\xi^2)\right),$$

while $\mathbf{v}_0$ and $\mathbf{v}_n$ are

$$\mathbf{v}_0=\frac{1}{2}\left(z_t(\mathbf{a}_{3t}-\mathbf{A}_{3t})+z_b(\mathbf{a}_{3b}-\mathbf{A}_{3b})\right)\qquad \mathbf{v}_n=\frac{1}{2}\left(z_t(\mathbf{a}_{3t}-\mathbf{A}_{3t})-z_b(\mathbf{a}_{3b}-\mathbf{A}_{3b})\right).$$

The displacement derivatives are then

$$\begin{cases} \mathbf{d}_{,\alpha} = \mathbf{d}^{u}_{,\alpha} + \mathbf{d}^{v}_{,\alpha} = \mathbf{u}_{0,\alpha} + \xi^3 \mathbf{u}_{n,\alpha} + \mathbf{v}_{0,\alpha} + \xi^3 \mathbf{v}_{n,\alpha} \\ \mathbf{d}_{,3} = \mathbf{d}^{u}_{,3} + \mathbf{d}^{v}_{,3} = \mathbf{u}_n + \mathbf{v}_n \end{cases} \tag{17}$$

Using Eq. (17), the covariant strains are expressed as the sum of 3 contributions

$$\bar{E}_{ij} = \bar{E}^{uu}_{ij} + \bar{E}^{vv}_{ij} + \bar{E}^{uv}_{ij} \tag{18}$$

where

$$\begin{cases} \bar{E}^{uu}_{ij} = \dfrac{1}{2}\left(\mathbf{X}_{,i}\cdot\mathbf{d}^{u}{}_{,j} + \mathbf{d}^{u}{}_{,i}\cdot\mathbf{X}_{,j} + \mathbf{d}^{u}{}_{,i}\cdot\mathbf{d}^{u}{}_{,j}\right), \\ \bar{E}^{vv}_{ij} = \dfrac{1}{2}\left(\mathbf{X}_{,i}\cdot\mathbf{d}^{v}{}_{,j} + \mathbf{d}^{v}{}_{,i}\cdot\mathbf{X}_{,j} + \mathbf{d}^{v}{}_{,i}\cdot\mathbf{d}^{v}{}_{,j}\right), \qquad i,j = 1\cdots 3 \\ \bar{E}^{uv}_{ij} = \dfrac{1}{2}\left(\mathbf{d}^{u}{}_{,i}\cdot\mathbf{d}^{v}{}_{,j} + \mathbf{d}^{v}{}_{,i}\cdot\mathbf{d}^{u}{}_{,j}\right), \end{cases} \tag{19}$$

By exploiting Eq.(2), the covariant strain components are collected in a Voigt notation in the vector $\bar{\mathbf{E}} = [\bar{E}_{11}, \bar{E}_{22}, 2\bar{E}_{12}, \bar{E}_{33}, 2\bar{E}_{23}, 2\bar{E}_{13}]^T$ and linearized with respect to ξ^3

$$\bar{\mathbf{E}} \approx \begin{bmatrix} \bar{\mathbf{e}}(\xi^1,\xi^2) + \xi^3\,\bar{\boldsymbol{\chi}}(\xi^1,\xi^2) \\ \bar{E}_{33}(\xi^1,\xi^2) \\ \bar{\boldsymbol{\gamma}}(\xi^1,\xi^2) \end{bmatrix} \tag{20}$$

where

$$\bar{\mathbf{e}}(\xi^1,\xi^2) = \begin{bmatrix} \bar{E}_{11}(\xi^1,\xi^2,0) \\ \bar{E}_{22}(\xi^1,\xi^2,0) \\ 2\bar{E}_{12}(\xi^1,\xi^2,0) \end{bmatrix}, \quad \bar{\boldsymbol{\chi}}(\xi^1,\xi^2) = \begin{bmatrix} \bar{E}_{11,3}(\xi^1,\xi^2,0) \\ \bar{E}_{22,3}(\xi^1,\xi^2,0) \\ 2\bar{E}_{12,3}(\xi^1,\xi^2,0) \end{bmatrix}, \quad \bar{\boldsymbol{\gamma}}(\xi^1,\xi^2) = \begin{bmatrix} 2\bar{E}_{23}(\xi^1,\xi^2,0) \\ 2\bar{E}_{13}(\xi^1,\xi^2,0) \end{bmatrix}. \tag{21}$$

The explicit expression for the covariant strain components, the definition of the strain energy and constitutive matrix of the layer in generalized quantities are defined in [25]

3 NOTES ON THE ISOGEOMETRIC FORMULATION AND SOLUTION METHOD

An isogeometric approximation, corresponding to that presented in [19], is adopted for each Kirchhoff-Love layer. The solid-shell layers do not require any discretization. The problem variables are then 3 for each control point of the Kirchhoff-Love layers. This means a minimal number of variables without accuracy loss since, in contrast to layer-wise or zigzag formulations [17], all the information of the 3D kinematics is maintained. The formulation has then the same level of accuracy as that proposed in [26] where a solid-shell model has been employed for all the layers but with a strong reduction in the number of DOFs.

A patch-wise numerical integration scheme [27, 28, 21] which uses a minimal number of integration points, allows to avoid locking effects and enhance the efficiency of the formulation. Details on the construction of the numerical model and the explicit expression of the operators for soft and hard layers can be found in [25]

The Riks arc-length method [29] is the general solution strategy used to trace these curves in a step-by-step manner from a known initial configuration. At each step some Newton iterations are needed to solve the equlibrium set of equations as detailed in [30]. Robustness and efficiency

of the iterative solution for displacement-based large deformation formulations are achieved by using the mixed integration point (MIP) strategy [30, 31, 32, 33, 34] for solids, shells and beams. This is particularly suitable for the considered problem.

4 NUMERICAL RESULTS

To validate the proposed modeling strategy, this section analyzes laminated structures experiencing buckling and/or large deflections. The numerical tests involve four distinct layups, representative of laminated glass. For brevity, these layups are described only once below.

- Layup $L3_A$: 3 alternating layers of which 2 glass layers of 4 mm with $E = 70$ GPa and $\nu = 0.23$ and 1 interlayer of 1.02 mm with $E = 1$ MPa and $\nu = 0.48$.
- Layup $L3_B$: 3 alternating layers of which 2 glass layers of 0.5 mm with $E = 70$ GPa and $\nu = 0.23$ and 1 interlayer of 2.04 mm with $E = 0.2$ MPa and $\nu = 0.48$.
- Layup $L5_A$: 5 alternating layers of which 3 glass layers of 12 mm with $E = 70$ GPa and $\nu = 0.23$ and 2 interlayers of 1.52 mm with $E = 5.96$ MPa and $\nu = 0.48$.
- Layup $L5_B$: 5 alternating layers of which 3 glass layers of 4 mm with $E = 70$ GPa and $\nu = 0.23$ and 2 interlayers of 1.02 mm with $E = 1$ MPa and $\nu = 0.48$.

The following 3 models compared:

- SS-KL: this proposal consisting in a Kirchoff-Love shell for each stiff layer and a solid-shell for the soft interlayers (DOFs per section $= 3 \times N_s$)
- SS: the reference solution based on full solid-shell model with one element per layer (DOFs per section $= 6 \times N_s$)
- KL-ZZ: the Kirchhoff-Love shell model hierarchically enriched with the zig-zag function [17] (DOFs per section = 5 regardless of the number of layers).

where N_s is the number of stiff layers. The same cubic C^2 NURBS interpolation are used for all the models.

This study considers a range of tests, from beams and plates to shells. The initial tests on flat beams and plates are used to validate the model for simple structures with well-understood behavior, aiding readers interested in implementing our model. Subsequent tests on curved beams and shells are conducted to examine whether the curved geometry can induce thickness strains in the interlayers, which could challenge the assumption of equal rotation of the stiff layers made by other models [17, 16, 26]. It's important to note that the model referred to as SS is a full layer-wise model that precisely replicates the 3D solution in terms of the load-displacement curve (see [26]) and is taken as the reference solution. The KL-ZZ model, while the most efficient approach for modeling sectional warping in these structures, provides similar predictions to other models for the flat tests, as already reported in [17]. However, KL-ZZ disregards interlayer thickness strain and enforces equal rotation of the stiff layers. We include KL-ZZ only in the curved structure tests, where it is expected to fail, thus highlighting the necessity of our new approach.

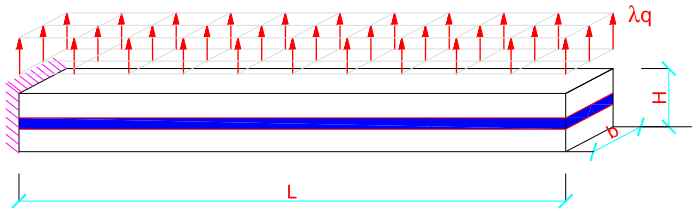

Figure 2: Cantilever beam under transverse load: geometry (mm), load, and boundary conditions.

4.1 Large deflection of a 3-layer cantilever beam loaded by a transverse distributed load

As first test is considered a laminated cantilever beam of length $L = 500$ mm subject to a distributed transversal load on the top glass layer as illustrated in Fig. 2. Are considered the stacking sequences $L3_A$ and $L3_B$. The surface load is $q = 10^{-2}$ MPa for $L3_A$ and $q = 10^{-4}$ MPa for $L3_B$. 8 elements along the beam axis and only 1 along the width are used.

Figure 3 presents the load factor vs. tip displacement equilibrium curve for the two layups, comparing the results from different models. Both axial and transverse components were monitored. An excellent agreement between the SS and SS-KL models is observed, even at large deformations. The results also align with those obtained using Abaqus with a fine mesh of 3D elements [26], demonstrating the accuracy of the SS-KL modeling approach. This method effectively reduces the number of unknowns while retaining 3D capabilities.

The deformed configurations obtained by the SS-KL model are shown in Figure 4, where the warping of the sections is evident due to significant shear strain in the interlayer, particularly for layup $L3_A$, along with nearly equal finite rotation of the glass layers. Figure 5 depicts the axial normal stress and transverse shear strain for layup $L3_A$, with the thickness dimension exaggerated to make the through-the-thickness variation visible. It can be seen that the shear strain is concentrated in the interlayer and varies significantly along the beam axis due to the end effect of the fully clamped boundary condition. Additionally, the normal stress exhibits a piecewise linear distribution, intermediate between a rigid section model and one with decoupled glass layers, highlighting the need for warped kinematics. For this test, the KL-ZZ shell model, enhanced with a zigzag function, also provides similar results due to the nearly equal rotation of the stiff layers [17].

4.2 5-layer rectangular plate under compression simply supported on 4 edges

The rectangular simply supported plate depicted in Fig. 6 is made of five alternating layers (layup $L5_A$) is now considered under two different loading cases: an out-of-plane load distributed over the plate and an axial compression load distributed on the glass surfaces of the short edges. The support is assigned on the border of the bottom layer and surface load of magnitude $q = 10^{-3}$ MPa for the transverse load case applied on the top layer, while a surface load distributed on glass layers of $q = 1$ MPa in the compression test is considered. For the second load case, a geometric imperfection shaped like the first linearized buckling mode, with a maximum deviation of 0.1, is introduced to guide the structure onto the bifurcated path. The equilibrium paths, shown in Fig. 7, exhibit large deflections and buckling under the two respective load conditions.

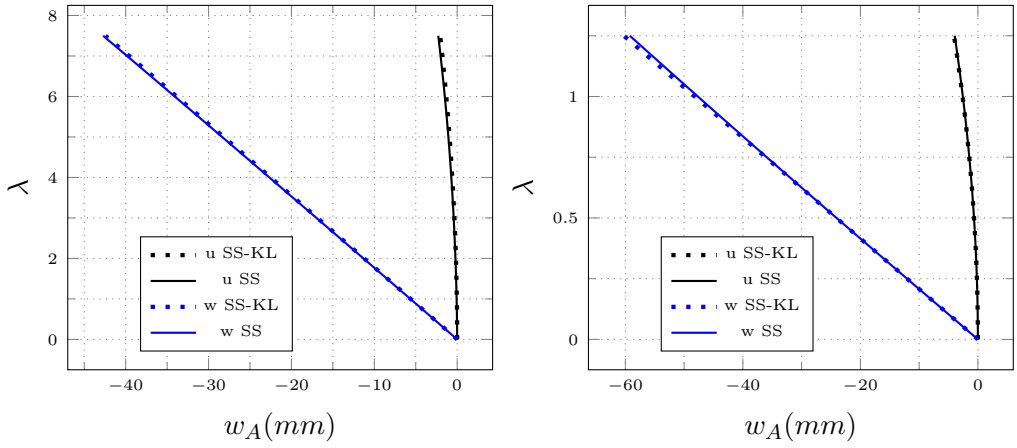

Layup $L3_A$ Layup $L3_B$

Figure 3: Cantilever beam under transverse load: comparison of the equilibrium path obtained by SS-KL and SS model.

Layup $L3_A$ SS-KL Layup $L3_A$ SS Layup $L3_B$ SS-KL Layup $L3_B$ SS

Figure 4: Cantilever beam under transverse load: deformed configuration at the last equilibrium point.

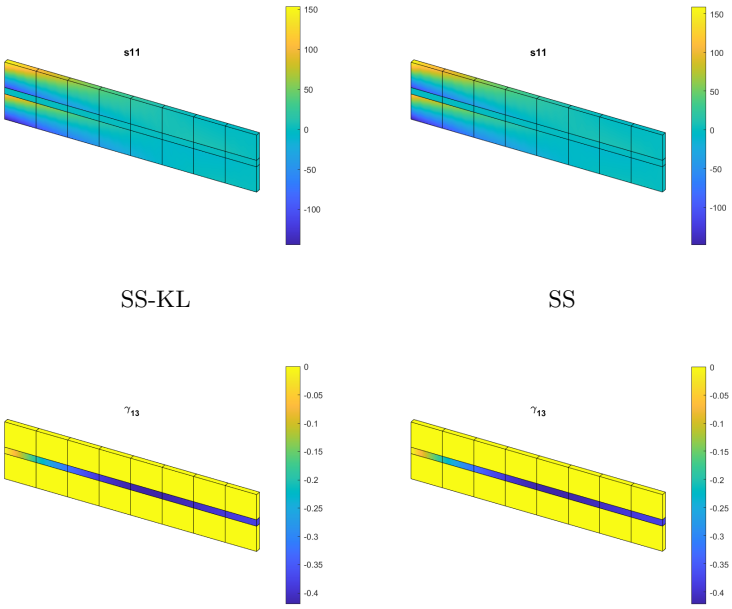

SS-KL SS

SS-KL SS

Figure 5: Cantilever beam under transverse load: normal stress σ_{11} (MPa), with 1 is the beam axis, and transverse shear strain γ_{13} for layup $L3_A$.

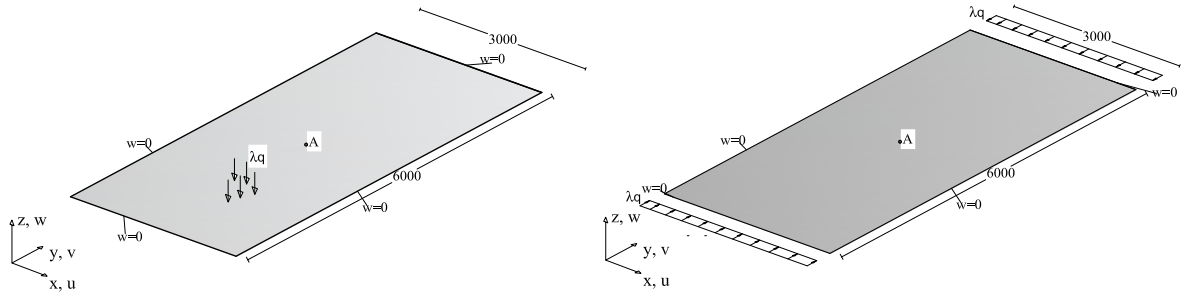

Transverse load Axial compression

Figure 6: Rectangular plate: geometry (mm), loads and boundary conditions.

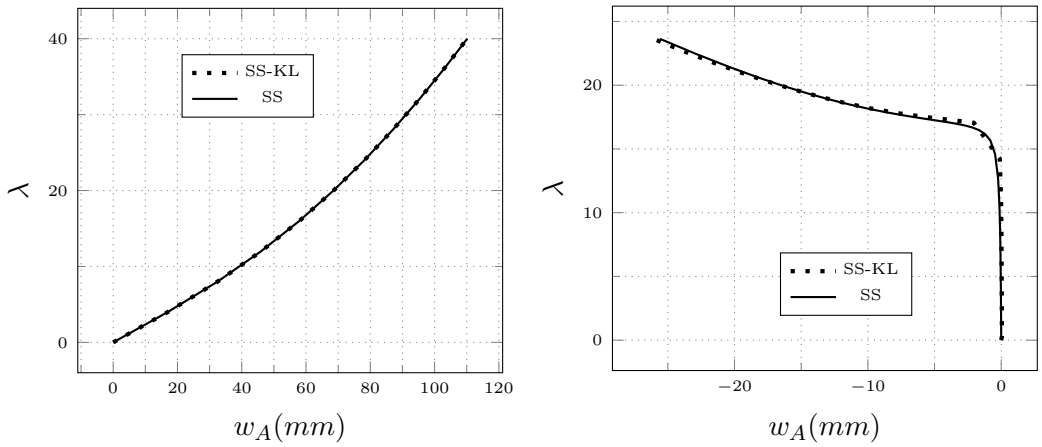

Figure 7: Rectangular plate: equilibrium path and comparison between SS-KL and SS model for the two load cases.

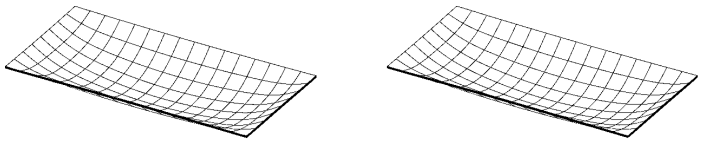

SS-KL SS

Figure 8: Rectangular plate under transverse load: deformed shape comparison between SS-KL and SS model.

The deformed configurations at the last equilibrium point are displayed in Fig. 8 and Fig. 9. The curves are presented for different models, once again demonstrating the accuracy of the proposed SS-KL finite element in this 5-layer case, achieving similar precision as the full SS model but with half the number of unknowns. The KL-ZZ shell model, enhanced with a zigzag function, also yields very close results, as reported in [17].

4.3 3-layer curved bar

The 3-layer curved cantilever bar depicted in Fig. 10, is analyzed in order to control the accuracy of the proposal for a structure with non-flat geometry. A transverse shear load of $q = 10^{-2}$ MPa is applied to the glass layers at the free end. The discretization used consists of 8×1 elements along the bar axis, with the layup $L3_A$ considered. The equilibrium path of the structure is depicted in Fig. 11, showing the out-of-plane displacement of one of the end nodes of the bar. In this initially curved case, it is evident that the KL-ZZ shell model, enhanced with a zigzag function, loses accuracy. This behavior, observed in many other curved structures, is due to the initial curvature combined with the large stiffness ratio of the materials, which induces a variable thickness strain, invalidating the assumption of equal rotation of the stiff layers. An

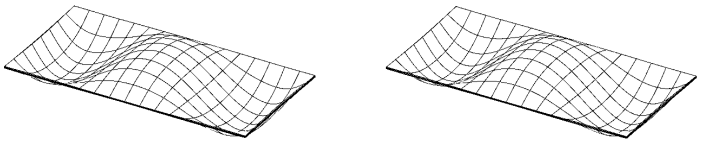

SS-KL SS

Figure 9: Rectangular plate under compression: deformed shape comparison between SS-KL and SS model.

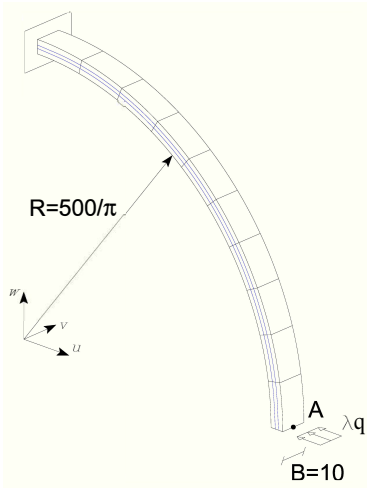

Figure 10: Curved bar: geometry (mm), loads and boundary conditions.

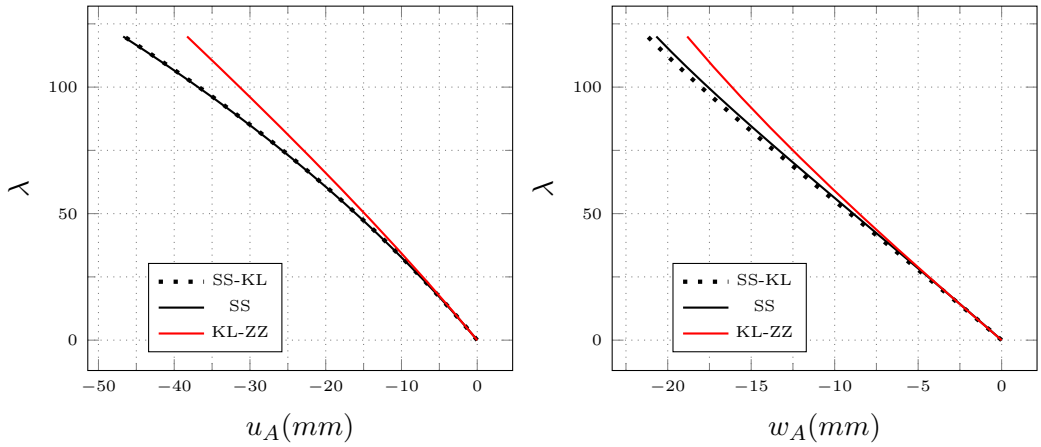

Figure 11: Curved bar: equilibrium path and comparison between SS-KL and SS models.

excellent match is achieved between our proposed model and the full SS solution, both of which account for this kinematic effect. Similar observations apply to the stress and strain fields shown in Fig. 12 for SS and SS-KL, with the thickness direction amplified for clearer visualization.

4.4 5-layer curved panel

In the test the curved shell with geometry of Fig. 14 is analyzed. The shell is simply supported vertically along the bottom curved edges and is subjected to an inward vertical load of 1 MPa distributed across the top surface of the laminate. The in-plane discretization used consists of 8×8 layered elements. The equilibrium path of the structure is shown in Fig. 15 for layup $L5_B$, depicting the vertical displacement of point A, located at the midpoint of the inner layer's straight edges. Even for small displacements, the prediction of the KL-SS shell model with a zigzag function deviates from the full SS solution due to the initial curvature of the structure. In contrast, an excellent match is achieved between our proposed model and the full SS solution. This consistency also applies to the stress and strain fields at the last equilibrium point, as shown in Fig. 16 for both the SS and SS-KL models, with the thickness direction amplified for better visualization.

5 CONCLUSIONS

Alternating laminates are a common type of composite structure composed of multiple stiff layers separated by soft interlayers. Numerous large-rotation shell theories have been developed to model the mechanics of these structures, often focusing on sectional zigzag warping. This paper offers an excellent balance between accuracy, robustness, and the number of degrees of freedom (DOFs). Models with fewer DOFs typically overlook the thickness variation in the interlayers and the distinct rotations of the stiff layers when the initial or deformed geometry becomes significantly curved. In contrast, the proposed approach requires only 3 DOFs per stiff layer at each surface point, maintaining 3D capability without compromising accuracy. Additionally, the formulation is purely displacement-based, eliminating the need to directly handle 3D finite rotations and shear correction factors.

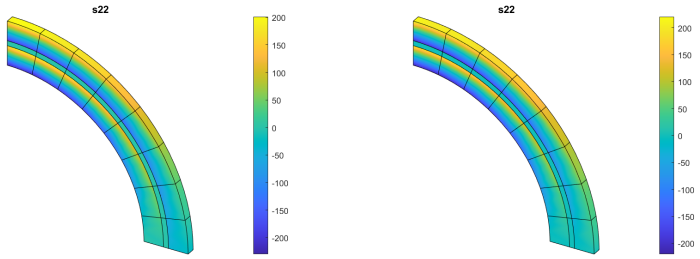

SS-KL SS

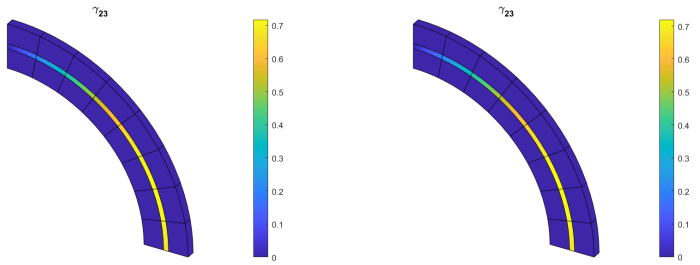

SS-KL SS

Figure 12: Curved bar: normal stress component σ_{22} (2 is the beam axis) and transverse shear strain component γ_{23} for $\lambda = 80$

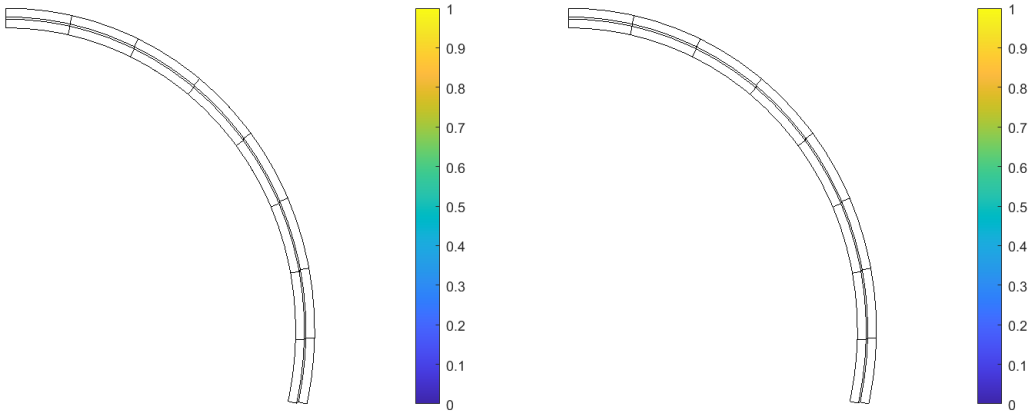

SS-KL SS

Figure 13: Curved bar: deformed shape for $\lambda = 80$.

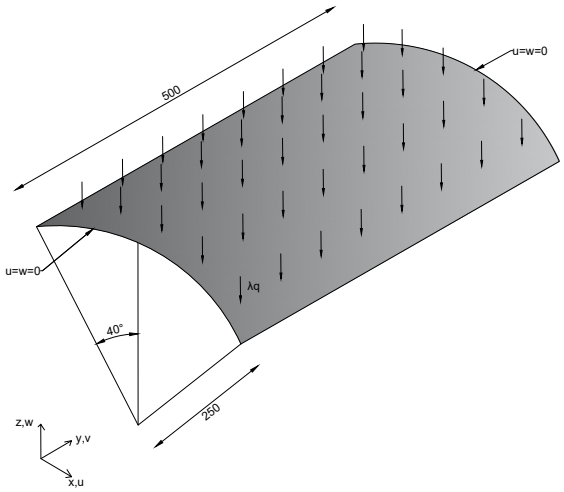

Figure 14: Curved panel: geometry (mm), loads, and boundary conditions.

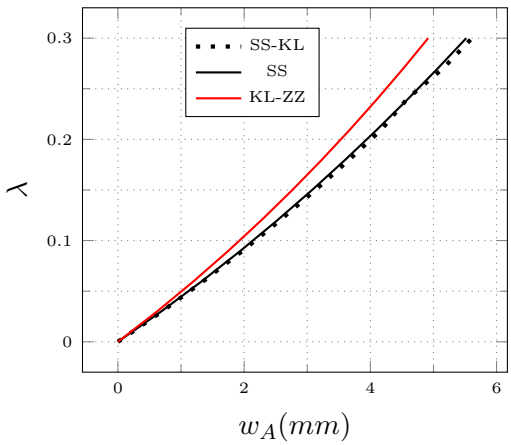

Figure 15: Curved panel: equilibrium path and comparison between SS-KL and SS models.

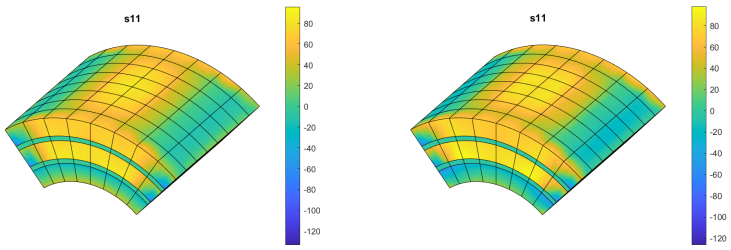

SS-KL SS

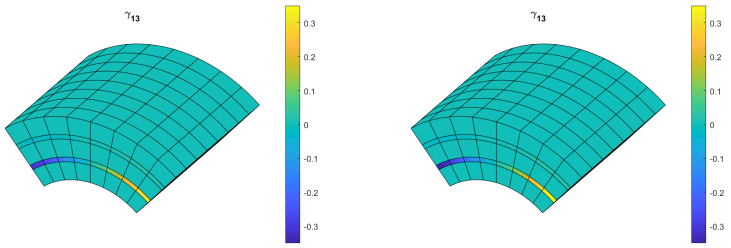

SS-KL SS

Figure 16: Curved panel: normal stress component σ_{11} (1 is the axis parallel to the straight edges) and transverse shear strain component γ_{13}.

REFERENCES

[1] Norville, H., King, K. & Swofford, J. Behavior and strength of laminated glass. *Journal Of Engineering Mechanics*. **124**, 46-53 (1998)

[2] Galuppi, L. & Royer-Carfagni, G. Shear coupling effects of the core in curved sandwich beams. *Composites Part B: Engineering*. **76** pp. 320-331 (2015)

[3] Haydar, A. & Royer-Carfagni, G. A Simple Model for Inflexed Multilayered Laminated Glass Beams Based on Refined Zig-Zag Theory. *Journal Of Applied Mechanics*. **90** (2022,10), 011002

[4] Reddy, J. On refined theories of composite laminates. *Meccanica*. **25** pp. 230-238 (1990)

[5] Cho, Y. & Averill, R. First-order zig-zag sublaminate plate theory and finite element model for laminated composite and sandwich panels. *Composite Structures*. **50**, 1-15 (2000)

[6] Demasi, L. Refined multilayered plate elements based on Murakami zig-zag functions. *Composite Structures*. **70**, 308-316 (2005)

[7] Gherlone, M., Tessler, A. & Sciuva, M. C0 beam elements based on the Refined Zigzag Theory for multilayered composite and sandwich laminates. *Composite Structures*. **93**, 2882-2894 (2011)

[8] Iurlaro, L., Gherlone, M., Di Sciuva, M. & Tessler, A. Assessment of the Refined Zigzag Theory for bending, vibration, and buckling of sandwich plates: a comparative study of different theories. *Composite Structures*. **106** pp. 777-792 (2013)

[9] Eijo, A., Onate, E. & Oller, S. A four-noded quadrilateral element for composite laminated plates/shells using the refined zigzag theory. *International Journal For Numerical Methods In Engineering*. **95**, 631-660 (2013)

[10] Flores, F. Implementation of the refined zigzag theory in shell elements with large displacements and rotations. *Composite Structures*. **118** pp. 560-570 (2014)

[11] Groh, R. & Tessler, A. Computationally efficient beam elements for accurate stresses in sandwich laminates and laminated composites with delaminations. *Computer Methods In Applied Mechanics And Engineering*. **320** pp. 369-395 (2017), https://www.sciencedirect.com/science/article/pii/S0045782516315602

[12] Reddy, J. Mechanics of Laminated Composite Plates and Shells: Theory and Analysis (2nd ed.). (CRC Press,2003)

[13] Ferreira, A., Fasshauer, G., Batra, R. & Rodrigues, J. Static deformations and vibration analysis of composite and sandwich plates using a layerwise theory and RBF-PS discretizations with optimal shape parameter. *Composite Structures*. **86**, 328-343 (2008)

[14] Thai, C., Ferreira, A., Carrera, E. & Nguyen-Xuan, H. Isogeometric analysis of laminated composite and sandwich plates using a layerwise deformation theory. *Composite Structures*. **104** pp. 196-214 (2013)

[15] Guo, Y. & Ruess, M. A layerwise isogeometric approach for NURBS-derived laminate composite shells. *Composite Structures.* **124** pp. 300-309 (2015)

[16] Liang, Y. & Izzuddin, B. Nonlinear analysis of laminated shells with alternating stiff/soft lay-up. *Composite Structures.* **133** pp. 1220-1236 (2015)

[17] Magisano, D., Corrado, A., Leonetti, L., Kiendl, J. & Garcea, G. Large deformation Kirchhoff-Love shell hierarchically enriched with warping: Isogeometric formulation and modeling of alternating stiff/soft layups. *Computer Methods In Applied Mechanics And Engineering.*

[18] Kiendl, J., Bletzinger, K., Linhard, J. & Wuchner, R. Isogeometric shell analysis with Kirchhoff-Love elements. *Computer Methods In Applied Mechanics And Engineering.* **198**, 3902-3914 (2009), https://www.sciencedirect.com/science/article/pii/S0045782509002680

[19] Leonetti, L., Magisano, D., Madeo, A., Garcea, G., Kiendl, J. & Reali, A. A simplified Kirchhoff-Love large deformation model for elastic shells and its effective isogeometric formulation. *Computer Methods In Applied Mechanics And Engineering.* **354** pp. 369 - 396 (2019)

[20] Leonetti, L. & Kiendl, J. A mixed integration point (MIP) formulation for hyperelastic Kirchhoff-Love shells for nonlinear static and dynamic analysis. *Computer Methods In Applied Mechanics And Engineering.* **416** pp. 116325 (2023), https://www.sciencedirect.com/science/article/pii/S0045782523004498

[21] Leonetti, L., Liguori, F., Magisano, D. & Garcea, G. An efficient isogeometric solid-shell formulation for geometrically nonlinear analysis of elastic shells. *Computer Methods In Applied Mechanics And Engineering.* **331** pp. 159 - 183 (2018)

[22] Magisano, D., Leonetti, L. & Garcea, G. Koiter asymptotic analysis of multilayered composite structures using mixed solid-shell finite elements. *Composite Structures.* **154** pp. 296-308 (2016)

[23] Liguori, F., Magisano, D., Leonetti, L. & Garcea, G. Nonlinear thermoelastic analysis of shell structures: solid-shell modelling and high-performing continuation method. *Composite Structures.* **266** pp. 113734 (2021) **418** pp. 116556 (2024), https://www.sciencedirect.com/science/article/pii/S0045782523006801

[24] Herrema, A., Johnson, E., Proserpio, D., Wu, M., Kiendl, J. & Hsu, M. Penalty coupling of non-matching isogeometric Kirchhoff-Love shell patches with application to composite wind turbine blades. *Computer Methods In Applied Mechanics And Engineering.* **346** pp. 810-840 (2019)

[25] Leonetti, L., Magisano, D. & Garcea, G. Large rotation isogeometric shell model for alternating stiff/soft curved laminates including warping and interlayer thickness change. *Computer Methods In Applied Mechanics And Engineering.* **424** pp. 116908 (2024), https://www.sciencedirect.com/science/article/pii/S0045782524001646

[26] Magisano, D., Leonetti, L., Garcea, G. & Royer-Carfagni, G. A constrained solid-shell model for the geometric nonlinear finite-element analysis of laminates with alternating stiff/soft layers. Applications to laminated glass. *International Journal Of Solids And Structures*. **274** pp. 112287 (2023), https://www.sciencedirect.com/science/article/pii/S0020768323001841

[27] Johannessen, K. Optimal quadrature for univariate and tensor product splines . *Computer Methods In Applied Mechanics And Engineering* . **316** pp. 84 - 99 (2017), Special Issue on Isogeometric Analysis: Progress and Challenges

[28] Adam, C., Hughes, T., Bouabdallah, S., Zarroug, M. & Maitournam, H. Selective and reduced numerical integrations for NURBS-based isogeometric analysis. *Computer Methods In Applied Mechanics And Engineering*. **284** pp. 732-761 (2015)

[29] Riks, E. An incremental approach to the solution of snapping and buckling problems. *International Journal Of Solids And Structures*. **15**, 529-551 (1979)

[30] Magisano, D., Leonetti, L. & Garcea, G. How to improve efficiency and robustness of the Newton method in geometrically non-linear structural problem discretized via displacement-based finite elements. *Computer Methods In Applied Mechanics And Engineering* . **313** pp. 986 - 1005 (2017)

[31] Magisano, D. & Corrado, A. New robust and efficient global iterations for large deformation finite element analysis of beams and shells with material nonlinearity. *Computer Methods In Applied Mechanics And Engineering*. **406** pp. 115900 (2023)

[32] Magisano, D., Leonetti, L., Madeo, A. & Garcea, G. A large rotation finite element analysis of 3D beams by incremental rotation vector and exact strain measure with all the desirable features. *Computer Methods In Applied Mechanics And Engineering*. **361** pp. 112811 (2020)

[33] Pfefferkorn, R., Bieber, S., Oesterle, B., Bischoff, M. & Betsch, P. Improving efficiency and robustness of enhanced assumed strain elements for nonlinear problems. *International Journal For Numerical Methods In Engineering*. **122**, 1911-1939 (2021)

[34] Leonetti, L. & Verhelst, H. A hierarchic isogeometric hyperelastic solid-shell. *Computational Mechanics*. pp. 1-20 (2024)